AEM JOURNAL.ORG

Coordinated EV Charging Pricing and Distributed Reactive Support for Secure High-Penetration Distribution Networks

Hongxi Wang*, Wei Huo, Peng Tao, Lei Chen, Guanghua Wu, Yuntong Lyu
Marketing Service Center of State Grid Hebei Electric Power Co., Ltd., Shijiazhuang 050000, China
Corresponding author: Hongxi Wang (e-mail: 19801559571@163.com).

ABSTRACT High-penetration electric-vehicle charging increasingly couples charging-service operation with distribution-network voltage security. However, existing pricing strategies often optimize user response or station profit separately from feeder-side voltage constraints. This paper proposes a coordinated rolling optimization method for station-wise EV charging pricing and distributed photovoltaic inverter reactive support in high-penetration source–load distribution networks. A utility-based probabilistic station-choice model captures user responses to charging cost, travel time, charging duration, and expected waiting time. A queue-aware charging-service simulator then updates charger occupation, queue carryover, and station-level charging loads over rolling intervals. These endogenous loads are mapped to distribution-network buses and evaluated using a second-order-cone branch-flow model with reactive support, enabling voltage-infeasible pricing decisions to be identified during optimization. A two-layer rolling procedure coordinates demand shaping and voltage support. Case studies show that pricing alone cannot restore feeder security during evening peaks. Compared with fixed pricing with reactive support, the proposed strategy increases operator profit by 37.74%, reduces expected waiting burden by 28.18%, lowers feeder losses by 9.03%, and reduces the station-load peak–valley gap by 24.46%. Results confirm that reactive support restores voltage feasibility, while dynamic pricing improves service and economic performance.

INDEX TERMS electric vehicle charging; dynamic pricing; source–load coordination; distribution network operation; photovoltaic inverter reactive support; second-order-cone optimal power flow

I. INTRODUCTION

Define The rapid growth of electric vehicles is changing the operating characteristics of urban distribution networks. EV ownership and public charging demand have increased steadily in many power systems, making charging infrastructure an important part of future urban energy systems [1], [2]. Public and semi-public fast-charging stations are also becoming larger and more spatially concentrated, especially in commercial areas, transport hubs, and urban corridors [3], [4]. Unlike conventional residential loads, EV charging demand is strongly affected by travel behavior, charging urgency, station accessibility, and price signals [5], [6]. When many users select the same charging stations during peak travel periods, charging demand may become highly concentrated in both time and space [3], [7]. Such concentration can increase waiting time at charging stations, reduce the balance of station utilization, and create additional stress on distribution feeders. Under high EV penetration, charging demand should therefore be understood as a service-side and grid-side coupling problem rather than a simple load-growth problem.

Traditional charging operation usually relies on fixed tariffs or simple time-of-use prices. Time-of-use pricing can encourage users to shift charging demand away from system peak periods, and it has been widely used in early EV demand-response studies [8]. However, fixed and time-segmented tariffs have limited ability to reflect real-time station congestion, charger availability, travel inconvenience, and local feeder conditions. User response to charging price can influence not only the total charging demand, but also the spatial distribution of charging loads among different stations [9], [10]. From the power-system perspective, the same total EV charging demand may lead to different voltage impacts depending on how it is allocated to feeder buses [11], [12]. Charging-service operation and distribution-network operation should therefore be coordinated rather than optimized as separate tasks.

A large body of research has investigated charging price design and demand-response strategies for EV charging systems. Dynamic pricing has been used to guide charging demand and improve station-level operating performance [9], [13]. Game-theoretic models, especially Stackelberg frameworks, have been adopted to describe the interaction between charging operators and EV users [10]. Reinforcement learning methods have also been introduced to learn pricing or scheduling policies under uncertain charging demand [13], [14]. Model predictive control has been applied to rolling charging management because it can update decisions as new system information becomes available [15]. Multi-agent optimization and distributed coordination methods have further been used when multiple stations, aggregators, or operators are involved [16], [17]. Pricing-based coordination methods have therefore become an important tool for improving charging-service operation at the service layer.

User behavior has also been introduced into charging-management studies. Utility-based models can represent the influence of charging cost, travel distance, charging duration, and station accessibility on user decisions [18]. Logit models and other probabilistic choice methods are widely used to describe heterogeneous station-selection behavior [19]. Queue-aware charging models consider the fact that users may avoid congested stations even when their prices are low [20]. Charging-service simulation has also been used to describe charger occupancy, service delay, and queue carryover between adjacent time intervals [21]. Behavioral charging models improve the realism of demand characterization and help explain why users may migrate from one station to another under price and queue signals.

However, most service-oriented pricing studies still focus mainly on charging operators or users. The feeder-side electrical constraints are often simplified, treated implicitly, or evaluated only after the charging strategy has been obtained. Some studies use aggregate EV load profiles to represent the effect of charging demand on the grid [22], [23], while others focus on price response without explicitly checking voltage feasibility at the distribution-network level [9], [18]. In such formulations, a price vector that reduces waiting time or increases operator profit may still move charging demand toward buses with limited voltage margin. Therefore, service-oriented charging strategies can improve operational efficiency, but their electrical feasibility under high charging penetration is not always guaranteed.

Distribution-network operation has been studied from a different perspective. Optimal power flow has been widely used to determine secure and economic operating points in active distribution networks [24]. Volt/Var optimization provides an effective way to regulate voltage profiles through reactive-power resources [25], [26]. For radial distribution systems, branch-flow formulations and second-order-cone programming relaxations have been developed to improve computational tractability while preserving the main structure of distribution power flow [27], [28]. SOCP-based feeder models are especially useful for rolling operation because feeder constraints need to be evaluated repeatedly under changing load and generation conditions. Grid-side optimization therefore provides the physical basis for secure operation.

Distributed inverter-based resources provide another important means for improving feeder security. Photovoltaic inverters can provide reactive power support when sufficient apparent-power margin is available [29], [30]. Flexible inverter control and PV-STATCOM operation have been studied for voltage regulation and hosting-capacity improvement in distribution networks [31]. Local reactive support can reduce voltage deviation and improve the ability of feeders to accommodate renewable generation and flexible loads [32]. In EV charging scenarios, inverter-based voltage support is particularly valuable because fast-charging stations may introduce large active-power demand during peak periods. Physical voltage support is therefore an important complement to demand-side charging coordination.

Although feeder-side optimization methods are effective for maintaining voltage security, they usually take the load profile as an input. EV charging demand is often assumed to be known before the feeder optimization is solved [33]. Such an assumption is convenient, but it misses an important feature of charging systems: station-level demand is not fixed. It is formed by user choices, queue conditions, charger availability, and price signals. If the feeder model does not describe how charging loads are formed, it cannot capture how a change in price may move demand from one station to another. Feeder-side control can determine whether a given load pattern is feasible, but it does not explain how that load pattern emerges from charging-service behavior.

Recent studies have started to combine transportation networks and distribution networks to better describe EV charging demand. Transportation–distribution coupling models can map travel demand, route choice, and charging-station locations to electrical loads [34], [35]. Agent-based simulation has been used to represent individual travel and charging behaviors [36]. Some studies further include station accessibility, detour time, and charging demand uncertainty in coupled traffic-power models [37]. Queue dynamics and waiting-time estimation have also been introduced to improve the realism of charging-load allocation. Existing transportation–distribution studies show that traffic-side information is important for understanding where and when EV charging loads appear.

Nevertheless, many transportation–distribution coupling models remain mostly one-directional. User trips and station choices are mapped to charging loads, and the loads are then imposed on the distribution network. Some studies consider traffic assignment and power-flow evaluation in the same framework [38], [39], while others combine station planning with distribution-network constraints [40], [41]. However, the feedback from feeder security to charging-service operation is still less developed. In particular, the closed-loop process from charging price to user response, from user response to load migration, and from load migration to voltage feasibility is not fully characterized. Such a process is central to high-penetration EV charging operation because price-guided load migration is useful only when the resulting feeder operating point remains secure.

The missing feedback between price-induced charging migration and feeder security motivates a coordinated formulation in which charging prices are not optimized only for service-side performance, and feeder operation is not evaluated with fixed EV charging profiles. In such a formulation, the charging-load pattern produced by user response should be tested against the voltage-feasible region of the feeder. At the same time, the role of pricing should be distinguished from that of physical voltage support. Pricing reshapes the spatial distribution of charging demand, whereas reactive support provides the electrical capability required to accommodate the resulting load pattern. A coordinated framework is therefore needed to connect user response, queue evolution, charging-load migration, and feeder-security evaluation within a rolling operation process.

This paper develops a coordinated rolling optimization framework for EV charging prices and distributed reactive support in a high-penetration source–load distribution network. The model connects utility-based station choice, queue-aware charging-service simulation, and SOCP-based feeder-security evaluation with station-oriented photovoltaic inverter reactive support. Charging payment, travel time, charging duration, and anticipated waiting time determine user station-choice probabilities, while charger availability is updated across rolling intervals to capture queue carryover. The resulting station-level charging demand is mapped to the feeder and tested against voltage-security constraints. In this formulation, inverter reactive support is not treated as a new device-level control method. It is used as the physical mechanism that restores the voltage-feasible operating region under stressed charging conditions. Dynamic pricing then reshapes charging demand within that recovered region to improve service quality and operator benefit. By distinguishing behavioral demand shaping from physical voltage support, the proposed model evaluates whether a price-induced charging-load pattern is profitable, service-efficient, and electrically secure.

The main contributions of this paper are summarized as follows.

1) A closed-loop source–load coordination framework is developed for high-penetration EV charging operation. Unlike conventional pricing models that evaluate feeder constraints after load allocation, the proposed framework connects station-wise price decisions, user response, charging-load migration, and feeder voltage feasibility within a rolling optimization process.
2) An endogenous station-load formation model is established by integrating utility-based station choice and queue-aware charging-service simulation. In this model, station-level charging demand is determined by charging payment, travel burden, charging duration, expected waiting time, and charger-state carryover, rather than being prescribed as a fixed exogenous load.
3) A feeder-security evaluation model based on second-order-cone branch-flow optimization is incorporated into the pricing decision process. The model uses distributed photovoltaic inverter reactive support to characterize the voltage-feasible operating region and penalizes price-induced load patterns that violate the 0.95–1.05 p.u. voltage-security requirement.
4) The different roles of dynamic pricing and distributed reactive support are explicitly distinguished. Reactive support is used to restore the physical voltage-feasible region under stressed charging conditions, while dynamic pricing reshapes charging demand within the recovered secure region to improve service quality, operator profit, and feeder-side performance.

The remainder of this paper is organized as follows. Section II presents the coupled transportation–charging–feeder structure. Section III formulates the user-behavior and queue-aware charging-service model. Section IV introduces the distribution-network operation model with distributed reactive support. Section V describes the coordinated optimization problem and rolling solution procedure. Section VI reports the case-study results and comparative analysis. Section VII concludes the paper.

II. SOURCE–LOAD COUPLING IN HIGH-PENETRATION DISTRIBUTION NETWORKS

This section presents the source–load coupling structure of the studied system. In a distribution network with high EV charging penetration and distributed PV resources, the charging demand is not a fixed passive load. It is affected by user mobility, station accessibility, station-wise prices, queue conditions, and feeder-side security constraints. Therefore, the transportation network, charging-service process, and distribution feeder are modeled as a coupled operating system.

A. COUPLED TRANSPORTATION–CHARGING–FEEDER STRUCTURE

The studied system contains three interacting subsystems: a transportation network, a charging-service system, and a radial distribution feeder. The transportation network is represented by

$$G^{tr} = (N^{tr}, A^{tr}) \tag{1}$$

where N^{tr} is the set of traffic nodes and A^{tr} is the set of road links. The charging-service system contains a set of charging stations.

$$S = \{1, 2, \dots, N_s\} \tag{2}$$

The distribution feeder is denoted by

$$G^{gr} = (N^{gr}, E^{gr}) \tag{3}$$

where N^{gr} is the set of feeder buses and E^{gr} is the set of radial branches. Each charging station $s \in S$ is mapped to a feeder bus $n(s) \in N^{gr}$. The mapping relationship is described by

$$A^{map}_{j,s} = \begin{cases} 1, & n(s) = j, \\ 0, & n(s) \neq j, \end{cases} \quad j \in N^{gr}, \; s \in S \tag{4}$$

The EV charging load injected into bus j is then

$$p_{j,t}^{EV} = \sum_{s \in S} A_{j,s}^{map} p_{s,t}^{EV} \tag{5}$$

where $p_{s,t}^{EV}$ is the charging load at station s during hour t. This equation is the physical interface between the charging-service layer and the feeder-operation layer. It shows how station-level charging demand is converted into bus-level electrical load.

Although the mapping is deterministic, the station load is endogenous. It is determined by the charging-price vector, user accessibility, expected waiting time, and charger availability. Therefore, the feeder does not receive a fixed EV load profile. Instead, it receives the result of a behavioral and service-side allocation process.

The total active demand at bus j is

$$p_{j,t}^{L} = p_{j,t}^{base} + p_{j,t}^{EV} \tag{6}$$

where $p_{j,t}^{base}$ is the baseline active load. In this study, EV charging is represented as active-power demand, while reactive-power regulation is provided by distributed PV inverters in the feeder layer.

B. SOURCE–LOAD INTERACTION AND FEEDER FEEDBACK

At each hour t, the operator publishes a station-wise charging price vector

$$\boldsymbol{\pi}_t = [\pi_{1,t}, \pi_{2,t}, \ldots, \pi_{N_s,t}]^T \tag{7}$$

The price vector affects users' perceived charging utilities and station-choice probabilities. The selected stations then determine station-level charging loads, which are further mapped to feeder buses. The source–load interaction can be expressed as

$$\boldsymbol{\pi}_t \rightarrow Pr(u \rightarrow s \mid t) \rightarrow p_{s,t}^{EV} \rightarrow p_{j,t}^{EV} \rightarrow \{V_{i,t}, L_t^{loss}, Q_{m,t}^{pv}\} \tag{8}$$

This chain indicates that the charging price does not regulate feeder voltage directly. Instead, it reshapes user-side station selection and changes the spatial distribution of charging demand. The resulting bus-level load is then evaluated by the feeder-side operation model. Therefore, dynamic pricing is a demand-shaping tool, while distributed reactive support is the physical voltage-support resource.

The coupled process can be written compactly as

$$\{V_{i,t}, L_t^{loss}, Q_{m,t}^{pv}\} = H[G(\boldsymbol{\pi}_t, \Omega_t)] \tag{9}$$

where $G(\cdot)$ denotes the user-response and charging-service process, $H(\cdot)$ denotes the feeder-side SOCP operation model, and Ω_t is the system state. This equation also clarifies the division of functions between the two control layers. The upper layer changes the spatial distribution of charging demand by adjusting station prices, while the lower layer determines whether the resulting load distribution can be supported by the feeder. If the lower-layer OPF is infeasible, the corresponding price vector is not a valid operating decision, even if it improves waiting time or operator profit. Therefore, feeder feasibility acts as a hard boundary for the charging-price search.

The electrically admissible price set is defined as

$$\Pi_t^{safe} = \{\boldsymbol{\pi}_t \mid \exists \Xi_t,\ 0.95 \le V_{i,t} \le 1.05,\ \forall i \in N^{gr}\} \tag{10}$$

where Ξ_t is the set of feeder-side decision variables. A price vector outside Π_t^{safe} is not acceptable because it leads to an infeasible or voltage-insecure feeder operating point.

C. ROLLING STATE TRANSITION

The coordinated operation is performed on an hourly rolling horizon. The system state at hour t is defined as

$$\Omega_t = \{SOC_{u,t}, loc_{u,t}, b_{s,k,t}, p_{j,t}^{base}, q_{j,t}^{base}, P_{m,t}^{pv}\} \tag{11}$$

where $SOC_{u,t}$ and $loc_{u,t}$ describe the mobility state of EV user u; $b_{s,k,t}$ is the next available time of charger k at station s; $p_{j,t}^{base}$ and $q_{j,t}^{base}$ are baseline feeder loads, and $P_{m,t}^{pv}$ is the PV active output.

The station charging load depends on both the current price and the inherited service state

$$p_{s,t}^{EV} = G_s(\boldsymbol{\pi}_t, \Omega_t) \tag{12}$$

After user response, queue update, and feeder evaluation, the system state evolves as

$$\Omega_{t+1} = F(\Omega_t, \boldsymbol{\pi}_t, D_t) \tag{13}$$

where D_t denotes the exogenous information during hour t, including trip arrivals, baseline load, and PV output.

The rolling state transition is essential because charging-service states are path-dependent. A station that is heavily selected in the current hour may leave several chargers occupied in the next hour, even if the next-hour price becomes less attractive. As a result, the effect of a price decision is not limited to the current period. It can propagate through queue carryover and change both service quality and feeder stress in later intervals. The rolling source–load coordination process is illustrated in Figure 1.

III. USER BEHAVIOR AND CHARGING-SERVICE MODEL

This section formulates how EV users select charging stations and how station-level charging loads are formed. The proposed model includes charging-candidate identification, utility-based station choice, and queue-aware service update. These components are required because EV charging demand depends on both behavioral response and station service states.

The purpose of the user-behavior model is not to predict every individual decision exactly, but to generate a realistic station-level charging allocation under price and queue signals. This is sufficient for the coordinated operation problem because the feeder is affected by aggregate station loads rather than by the identity of individual users. The model therefore focuses on the probability of station selection, the resulting queue state, and the charging load formed at each station.

AEM JOURNAL .ORG

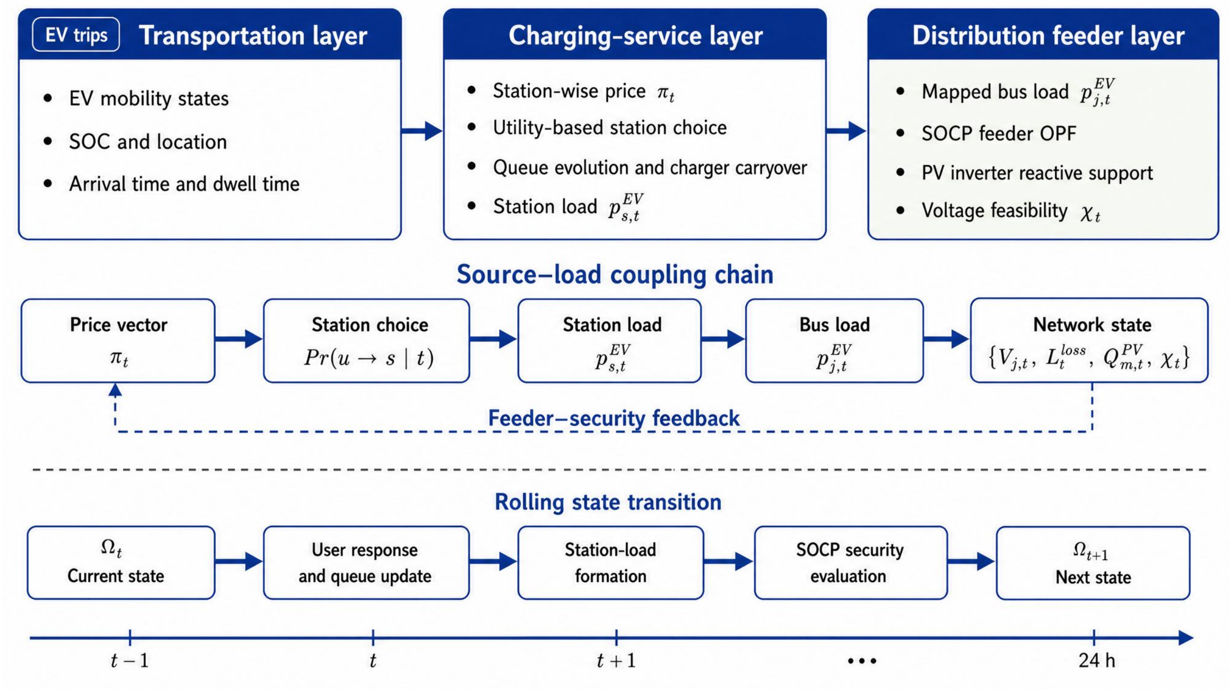

FIGURE 1. Rolling source–load coordination and state-transition process over the daily operation horizon.

A. CHARGING CANDIDATE AND FEASIBLE STATION SET

For user u, the charging decision is evaluated after the completion of a trip. The user becomes a charging candidate if the arrival SOC is lower than the charging threshold:

$$SOC^{arr}_{u,t} \leq SOC^{th} \tag{14}$$

For a candidate user, the required charging energy at station s is

$$E^{ch}_{u,s,t} = E^{max}[SOC^{tar} - SOC^{arr}_{u,t}]^{+} \tag{15}$$

where E^{max} is the battery capacity, SOC^{tar} is the target SOC, and $[x]^{+} = \max(x, 0)$.

The corresponding charging duration is

$$T^{ch}_{u,s,t} = \frac{E^{ch}_{u,s,t}}{P^{ch}_{s}} \tag{16}$$

where P^{ch}_{s} is the charging power of station s.

Not every station is feasible for every user. A feasible station must satisfy reachability and dwell-time constraints. Therefore, the feasible station set is defined as

$$S^{feas}_{u,t} = \left\{ s \in S \;\middle|\; \begin{array}{l} SOC^{arr}_{u,t} - \dfrac{E^{tr}_{u,s,t}}{E^{max}} \geq SOC^{min}, \\ T^{dwell}_{u,t} \geq T^{tr}_{u,s,t} + T^{ch}_{u,s,t} + W^{est}_{u,s,t} \end{array} \right\} \tag{17}$$

The first condition ensures that the user can physically reach the station, while the second condition ensures that the user can finish charging before the next trip. This feasibility filter prevents unrealistic charging assignments.

The feasible station set plays a screening role before the utility comparison is made. Without this screening, the model may assign users to stations that are attractive in price but infeasible in mobility. By combining SOC reachability and dwell-time constraints, the model ensures that the station-choice process remains consistent with the travel requirements of EV users.

B. GENERALIZED UTILITY AND PROBABILISTIC STATION CHOICE

For each feasible station, the user compares dimensionless charging burdens rather than directly mixing variables with different physical units. The normalized burden terms are defined as

$$\begin{cases} \widehat{C}_{u,s,t} = \dfrac{C_{u,s,t}}{C^{ref}}, & \widehat{T}^{tr}_{u,s,t} = \dfrac{T^{tr}_{u,s,t}}{T^{ref}}, \\ \widehat{T}^{ch}_{u,s,t} = \dfrac{T^{ch}_{u,s,t}}{\tau^{ref}}, & \widehat{W}^{est}_{u,s,t} = \dfrac{W^{est}_{u,s,t}}{W^{ref}} \end{cases} \tag{18}$$

where C^{ref}, T^{ref}, τ^{ref}, and W^{ref} are positive reference quantities used to non-dimensionalize charging payment, travel time, charging duration, and expected waiting time, respectively.

The dimensionless generalized charging utility is then written as

$$U_{u,s,t} = -\left(a_p\widehat{C}_{u,s,t} + a_\tau\widehat{T}^{tr}_{u,s,t} + a_e\widehat{T}^{ch}_{u,s,t} + a_w\widehat{W}^{est}_{u,s,t}\right) \tag{19}$$

Therefore, a higher charging payment, longer detour time, longer charging duration, or larger expected waiting burden decreases the perceived attractiveness of a charging station.

The charging payment is

$$C_{u,s,t} = \pi_{s,t}E^{ch}_{u,s,t} \tag{20}$$

The expected waiting time is estimated according to the current charger availability:

$$W_{u,s,t}^{est} = \left[\min_{k \in K_s} b_{s,k,t} - a_{u,s,t}\right]^+ + \tau^{svc} \tag{21}$$

where $a_{u,s,t}$ is the arrival time of user u at station s; $b_{s,k,t}$ is the next available time of charger k; τ^{svc} is a fixed service buffer.

The normalized representation in (19) is fully equivalent to the signed linear form used in the implementation. The coefficient correspondence is

$$\begin{cases} \beta_p = -\dfrac{a_p}{C^{ref}}, & \beta_\tau = -\dfrac{a_\tau}{T^{ref}}, \\ \beta_e = -\dfrac{a_e}{\tau^{ref}}, & \beta_w = -\dfrac{a_w}{W^{ref}} \end{cases} \tag{22}$$

Therefore, the dimensionless utility model preserves the same behavioral logic as the simulation code while avoiding direct mixing of quantities with different units.

The station-choice probability is modeled using a logit rule:

$$Pr(u \to s \mid t) = \frac{\exp(U_{u,s,t})}{\sum_{r \in S_{u,t}^{feas}} \exp(U_{u,r,t})}, \quad s \in S_{u,t}^{feas} \tag{23}$$

The probabilities satisfy

$$\sum_{s \in S_{u,t}^{feas}} Pr(u \to s \mid t) = 1 \tag{24}$$

The logit formulation allows users with the same feasible station set to make different choices. This avoids the unrealistic outcome that all users select the same seemingly cheapest station. In addition, the utility includes expected waiting time, so congestion can reduce station attractiveness even when the charging price is relatively low. This feature is necessary for capturing the interaction between price guidance and queue pressure.

C. QUEUE-AWARE SERVICE UPDATE AND LOAD FORMATION

After a station is selected, the user is assigned to the earliest available charger:

$$k^* = \arg\min_{k \in K_s} b_{s,k,t} \tag{25}$$

The actual charging start time is

$$\widehat{a}_{u,s,t} = \max(a_{u,s,t}, b_{s,k^*,t}) \tag{26}$$

The realized waiting time is

$$W_{u,s,t}^{real} = \widehat{a}_{u,s,t} - a_{u,s,t} + \tau^{svc} \tag{27}$$

The charger release time is updated as

$$b_{s,k^*,t}^{new} = \widehat{a}_{u,s,t} + T_{u,s,t}^{ch} + \tau^{svc} \tag{28}$$

The queue update converts user arrivals into charger occupancy states. This process is important because waiting time is not prescribed externally. It is generated by the interaction between user arrivals and finite charging resources. Therefore, the model can capture both immediate congestion and delayed congestion caused by charging sessions that extend into later periods.

If $b_{s,k^*,t}^{new} > t + \Delta t$, the occupied charger state is carried into the next hour. This queue carryover creates temporal coupling between adjacent operating intervals.

Let $x_{u,s,t}$ denote the realized station-selection variable:

$$x_{u,s,t} = \begin{cases} 1, & \text{user } u \text{ selects station } s, \\ 0, & \text{otherwise} \end{cases} \tag{29}$$

Then the station-level charging energy is

$$E_{s,t}^{EV} = \sum_{u \in U_t^{ch}} x_{u,s,t} E_{u,s,t}^{ch} \tag{30}$$

The corresponding station-level charging load is

$$p_{s,t}^{EV} = \frac{E_{s,t}^{EV}}{\Delta t} \tag{31}$$

The average waiting time is

$$W_t = \frac{\sum_{u \in U_t^{serve}} W_{u,t}^{real}}{|U_t^{serve}|} \tag{32}$$

The station-load peak–valley disparity is

$$\Delta_t^{pv} = \max_{s \in S} p_{s,t}^{EV} - \min_{s \in S} p_{s,t}^{EV} \tag{33}$$

The operator profit is

$$\Pi_t = \sum_{s \in S} \pi_{s,t} E_{s,t}^{EV} - c_t^{grid} \sum_{s \in S} E_{s,t}^{EV} \tag{34}$$

These service-side indicators are later used to evaluate different price strategies. Average waiting time reflects user convenience, station-load disparity reflects spatial concentration of charging demand, and operator profit reflects the economic viability of the pricing decision. Together, they describe whether a price vector improves charging-service operation before the feeder-side security check is considered. The complete user-choice and queue-aware service process is shown in Figure 2.

IV. DISTRIBUTION-NETWORK OPERATION MODEL

This section formulates the feeder-side secure-operation model. The station-level EV load is mapped to feeder buses, and the lower layer determines whether voltage security can be maintained with distributed PV inverter reactive support. The model is based on the branch-flow formulation and SOCP relaxation for radial distribution networks.

The feeder-side model is introduced to ensure that the charging-load distribution produced by the upper layer is electrically feasible. In the studied high-penetration setting, voltage security cannot be guaranteed by price guidance alone. Local reactive support from distributed PV inverters is therefore embedded into the OPF model to recover the secure operating region under stressed charging conditions.

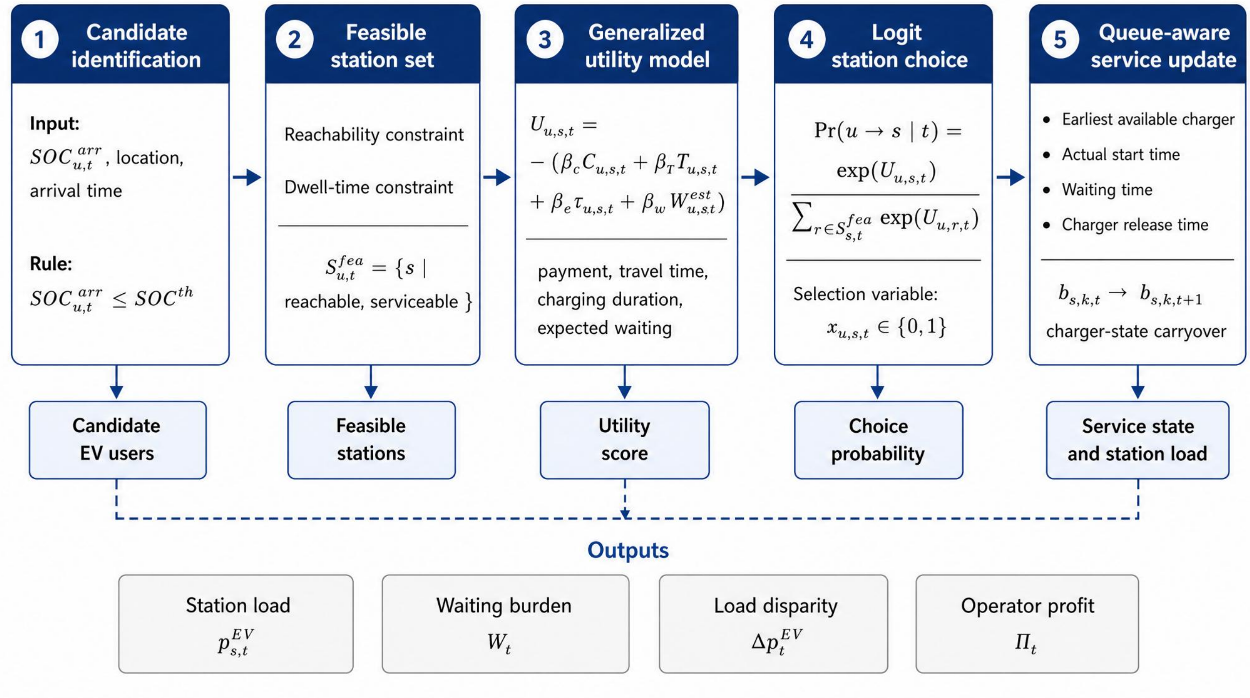

FIGURE 2. Utility-based station choice and queue-aware charging-service process for EV users.

A. NET LOAD AND PV INVERTER REACTIVE SUPPORT

The bus-level EV charging load is obtained as

$$p_{j,t}^{EV} = \sum_{s \in S} A_{j,s}^{map} p_{s,t}^{EV} \tag{35}$$

The net active load at bus j is

$$p_{j,t}^{net} = p_{j,t}^{base} + p_{j,t}^{EV} - \sum_{m \in M: m=j} P_{m,t}^{pv} \tag{36}$$

The net reactive load is

$$q_{j,t}^{net} = q_{j,t}^{base} - \sum_{m \in M: m=j} Q_{m,t}^{pv} \tag{37}$$

where M is the set of PV inverter support buses; $P_{m,t}^{pv}$ is the active PV output; $Q_{m,t}^{pv}$ is the inverter reactive output. The active PV output is treated as an exogenous profile, while the reactive output is optimized for voltage support.

The inverter apparent-power constraint is

$$(P_{m,t}^{pv})^2 + (Q_{m,t}^{pv})^2 \le (S_m^{inv})^2, \quad m \in M \tag{38}$$

The feasible reactive-power range is

$$-\sqrt{(S_m^{inv})^2 - (P_{m,t}^{pv})^2} \le Q_{m,t}^{pv} \le \sqrt{(S_m^{inv})^2 - (P_{m,t}^{pv})^2} \tag{39}$$

The inverter capability constraint links active PV output and available reactive support. When active PV generation is high, less inverter capacity remains for reactive regulation. When active PV generation is low, more capacity can be used for reactive support. This relationship is particularly relevant in evening charging periods, when EV demand remains high but PV active output may decrease.

B. SOCP BRANCH-FLOW FORMULATION

For branch $(i,j) \in E^{gr}$, the active and reactive branch-flow equations are

$$P_{ij,t} = \sum_{m:(j,m) \in E^{gr}} P_{jm,t} + p_{j,t}^{net} + r_{ij} \ell_{ij,t} \tag{40}$$

$$Q_{ij,t} = \sum_{m:(j,m) \in E^{gr}} Q_{jm,t} + q_{j,t}^{net} + x_{ij} \ell_{ij,t} \tag{41}$$

The squared-voltage equation is

$$v_{j,t} = v_{i,t} - 2(r_{ij} P_{ij,t} + x_{ij} Q_{ij,t}) + (r_{ij}^2 + x_{ij}^2) \ell_{ij,t} \tag{42}$$

The original nonlinear current-power relation is

$$P_{ij,t}^2 + Q_{ij,t}^2 = v_{i,t} \ell_{ij,t} \tag{43}$$

To obtain a convex lower-layer problem, this relation is relaxed as

$$\left\| \begin{bmatrix} 2P_{ij,t} \\ 2Q_{ij,t} \\ \ell_{ij,t} - v_{i,t} \end{bmatrix} \right\|_2 \le \ell_{ij,t} + v_{i,t} \tag{44}$$

The branch-current limit is

$$0 \le \ell_{ij,t} \le \bar{I}_{ij}^2 \tag{45}$$

The SOCP relaxation keeps the branch-flow structure while making the lower-layer problem computationally tractable. This is important for the rolling framework because the feeder model must be solved repeatedly for different price candidates. The objective is not to develop a new power-flow relaxation method, but to provide a reliable and efficient feeder-security check within the coordinated operation model.

C. VOLTAGE SECURITY AND FEEDER-SIDE EVALUATION

The feeder voltage must remain within the secure operating range:

$$0.95 \le V_{i,t} \le 1.05, \quad \forall i \in N^{gr} \tag{46}$$

In squared-voltage form, this becomes

$$0.95^2 \le v_{i,t} \le 1.05^2 \tag{47}$$

The feeder loss is

$$L_t^{loss} = \sum_{(i,j)\in E^{gr}} r_{ij}\ell_{ij,t} \tag{48}$$

The voltage-deviation severity is

$$V_t^{dev} = \sum_{i\in N^{gr}} (V_{i,t} - 1)^2 \tag{49}$$

The lower-layer OPF is formulated as

$$\min_{\Xi_t} \ \alpha_l L_t^{loss} + \alpha_v V_t^{dev} + \alpha_q \sum_{m\in M} (Q_{m,t}^{pv})^2 \tag{50}$$

Subject to the net-load equations, branch-flow equations, SOCP constraints, inverter-capability constraints, and voltage-security constraints.

The lower-layer decision-variable set is

$$\Xi_t = \{P_{ij,t}, Q_{ij,t}, \ell_{ij,t}, v_{i,t}, Q_{m,t}^{pv}\} \tag{51}$$

The feeder feasibility flag is defined as

$$\chi_t = \begin{cases} 1, & \text{SOCP OPF is feasible,} \\ 0, & \text{SOCP OPF is infeasible} \end{cases} \tag{52}$$

If the OPF is infeasible, the corresponding upper-layer price candidate is penalized:

$$J_t^{pen} = J_t + M(1 - \chi_t) \tag{53}$$

where M is a large penalty coefficient.

The feasibility penalty prevents the upper layer from selecting price vectors that perform well in service-side indicators but violate feeder security. This is the key link between the behavioral layer and the electrical layer. The final charging-price decision must therefore satisfy both service-side objectives and feeder-side voltage constraints. The distribution-network operation model is shown in Figure 3.

V. COORDINATED OPTIMIZATION AND SOLUTION PROCEDURE

This section formulates the coordinated rolling optimization problem. The upper layer determines station-wise charging prices, whereas the lower layer evaluates whether the resulting charging-load pattern can be securely operated with feeder-side support. The overall problem is simulation-coupled and nonconvex because user choice and queue evolution are embedded in the objective, while the lower-layer feeder problem is convex after SOCP relaxation.

The coordinated optimization structure is shown in Figure 4. The upper layer generates station-wise price candidates, while the lower layer evaluates whether the resulting charging-load pattern can be securely operated with PV inverter reactive support.

A. UPPER-LAYER DYNAMIC PRICING MODEL

The upper layer minimizes a normalized objective function that combines service-side, economic, and feeder-side performance indicators. The objective is written as

$$\begin{aligned}\min_{\boldsymbol{\pi}_t} J_t = {} & w_W \widehat{W}_t - w_\Pi \widehat{\Pi}_t + w_\Delta \widehat{\Delta}_t^{pv} \\ & + w_L \widehat{L}_t^{loss} + w_V \widehat{V}_t^{dev} + M(1 - \chi_t)\end{aligned} \tag{54}$$

where w_W, w_Π, w_Δ, w_L, and w_V are the weights assigned to the expected waiting burden, operator profit, station-load peak–valley disparity, feeder loss, and voltage-deviation severity, respectively. The term $M(1 - \chi_t)$ is a feasibility-penalty term, where M is a sufficiently large positive coefficient. When the lower-layer OPF is feasible, $\chi_t = 1$, and the penalty term is inactive. When the lower-layer OPF is infeasible, $\chi_t = 0$, and the candidate price vector is strongly penalized.

The normalized performance indicators are given by

$$\widehat{W}_t = \frac{W_t}{W^{ref}}, \quad \widehat{\Pi}_t = \frac{\Pi_t}{\Pi^{ref}}, \quad \widehat{\Delta}_t^{pv} = \frac{\Delta_t^{pv}}{\Delta^{ref}} \tag{55}$$

$$\widehat{L}_t^{loss} = \frac{L_t^{loss}}{L^{ref}}, \quad \widehat{V}_t^{dev} = \frac{V_t^{dev}}{V^{ref}} \tag{56}$$

The profit term is assigned a negative sign because the problem is formulated as a minimization problem, whereas a higher operator profit is desirable. The waiting-burden term reflects service quality from the user side. The station-load disparity term discourages excessive concentration of charging demand at a small number of stations. The feeder-loss and voltage-deviation terms encourage price-induced load distributions that are more favorable to feeder operation.

The station-wise price bounds are imposed as

$$\pi_s^{min} \le \pi_{s,t} \le \pi_s^{max}, \quad s \in S \tag{57}$$

When tariff smoothness between adjacent rolling intervals is required, the following ramping constraint can be added:

$$|\pi_{s,t} - \pi_{s,t-1}| \le \Delta\pi_s^{max} \tag{58}$$

This ramping constraint is optional and can be removed when the focus is on hourly operational feasibility and performance rather than on tariff continuity.

B. LOWER-LAYER FEEDER-SECURITY EVALUATION

For each candidate price vector generated by the upper layer, the lower layer evaluates whether the corresponding charging-load pattern can be operated securely in the distribution network. The lower layer receives the bus-level EV charging loads after station-to-bus mapping, together with the baseline load and PV active output. It then solves the

AEM JOURNAL.ORG

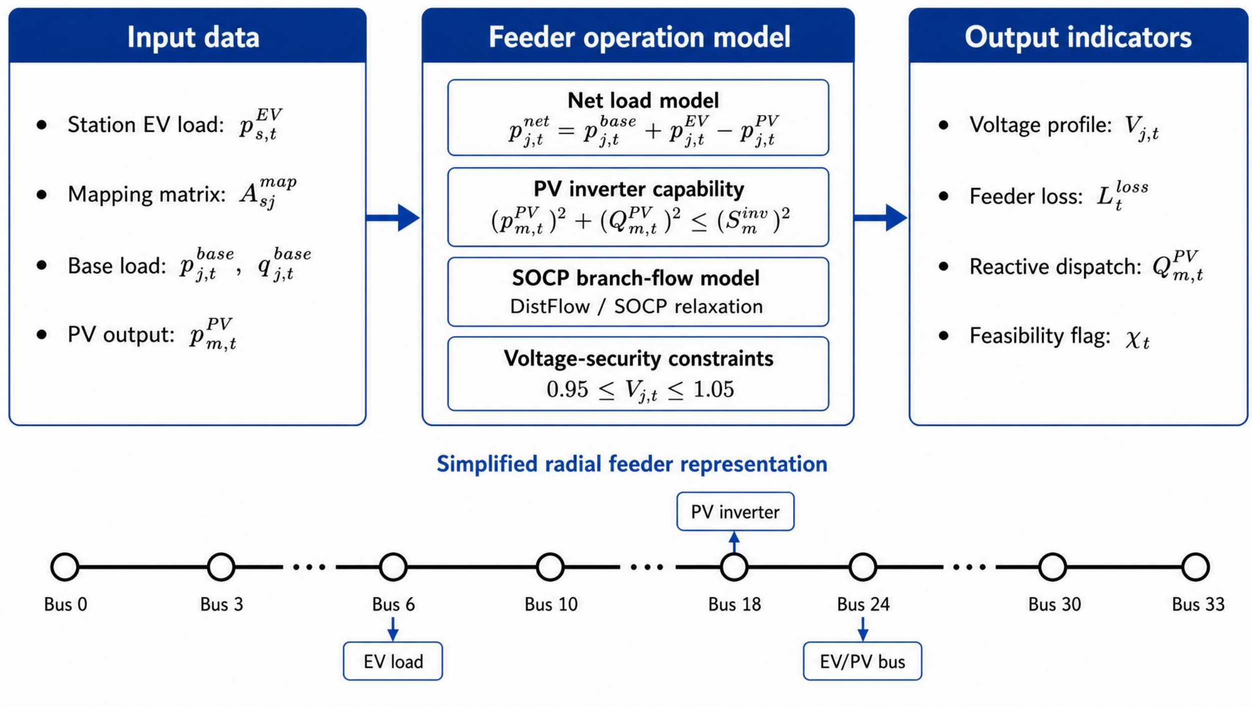

FIGURE 3. Distribution-network operation model with mapped EV charging loads and PV inverter reactive support.

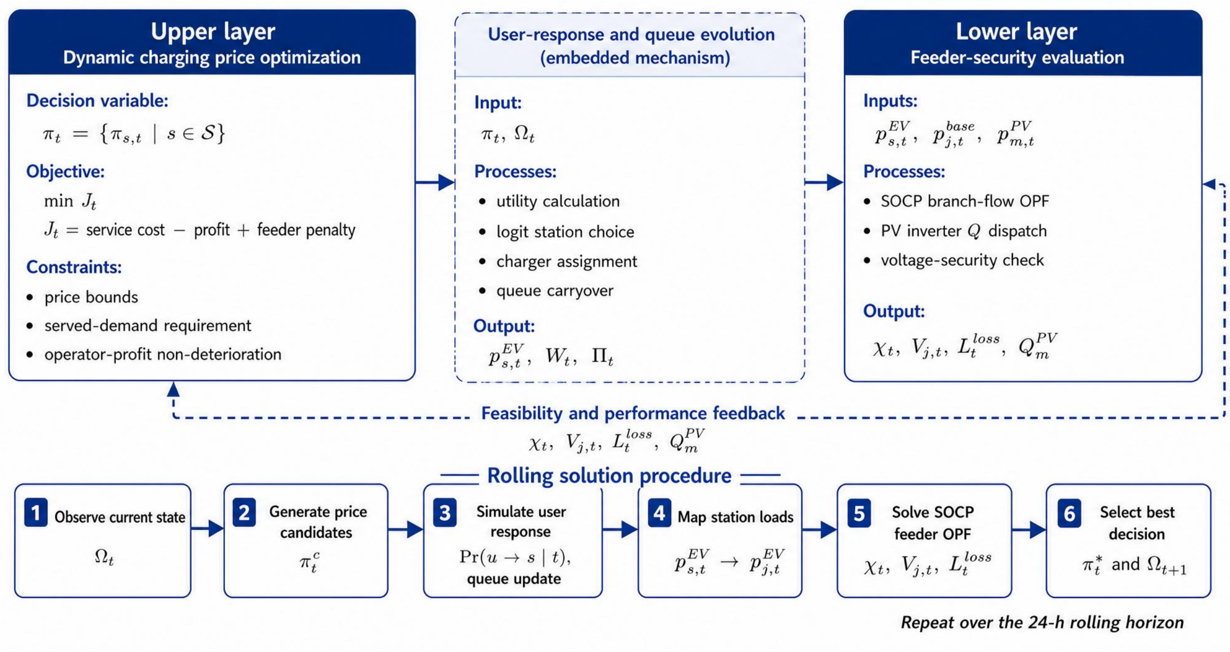

FIGURE 4. Two-layer coordinated optimization structure linking dynamic charging-price decisions and feeder-secure operation.

SOCP-based feeder OPF with PV inverter reactive-power support.

The lower layer serves two functions. First, it determines the feasibility of the price-induced charging-load pattern under the strict voltage-security requirement. Second, when the operating point is feasible, it provides feeder-side performance indicators, including feeder loss, voltage-deviation severity, and reactive-power dispatch. These indicators are returned to the upper layer and incorporated into the objective function.

This design avoids the weakness of an ex-post feasibility check. If feeder constraints were evaluated only after the pricing decision was obtained, the optimized price might shift charging demand toward electrically weak buses and cause voltage violations. In the proposed procedure, infeasible load patterns are identified during the search process. Therefore, the final selected price vector is shaped by both charging-service performance and feeder-security admissibility.

The penalized objective value used for candidate comparison can be written as

$$J_t^{pen} = J_t + M(1 - \chi_t) \tag{59}$$

where J_t is the normalized objective value before the feasibility penalty is applied. A feasible candidate satisfies $\chi_t = 1$, so that $J_t^{pen} = J_t$. An infeasible candidate satisfies $\chi_t = 0$, and its objective value is increased by M. This penalty mechanism allows the derivative-free upper-layer search to treat feeder infeasibility as part of the candidate evaluation.

C. ROLLING SOLUTION PROCEDURE

The proposed rolling procedure is summarized in Algorithm 1. The algorithm is executed sequentially over the daily operating horizon. At each hour, the current system state is observed, candidate price vectors are generated, and each candidate is evaluated through the coupled service-grid model. The selected price is then implemented, and the system state is updated for the next rolling interval.

VI. CASE STUDY

The test system consists of a 29-node transportation network, 11 charging stations, and an IEEE 33-bus radial distribution feeder, as shown in Figure 5. The transportation-side dataset contains 25,527 trip records. EV battery capacity is set to 60 kWh, and the target SOC is set to 0.9. The behavioral coefficients used in the station-choice model are $\beta_p = -1.2$, $\beta_\tau = -0.7$, $\beta_e = -0.2$, and $\beta_w = -0.5$. These coefficients describe the relative effects of charging payment, travel time, charging duration, and expected waiting burden on station-selection utility.

The distribution feeder is constrained by the voltage-security range of 0.95–1.05 p.u. Six PV units are connected at buses 18, 22, 24, 29, 30, and 32. The rated active power of each PV unit is 1500 kW, and the inverter rating is 2250 kVA. The inverter reactive-power capability is used as the distributed voltage-support resource. Night-time reactive support is enabled in the studied setting. The main system parameters are summarized in Table I.

A. FEASIBILITY RESTORATION BY DISTRIBUTED REACTIVE SUPPORT

To distinguish the roles of charging pricing and reactive support, four benchmark cases are constructed. The first two cases do not include reactive support, while the last two cases include PV inverter reactive-power dispatch. This design allows the feasibility-restoration role of reactive support and the performance-improvement role of coordinated pricing to be evaluated separately.

C1 uses fixed charging prices without reactive support. C2 uses optimized station-wise charging prices without reactive support. C3 uses fixed charging prices with PV inverter reactive support. C4 uses optimized station-wise charging prices with PV inverter reactive support. The four-case comparison shows that both no-support cases are infeasible in the representative evening hours under the 0.95–1.05 p.u. voltage constraint. This result is important because it shows that pricing alone cannot guarantee feeder security in the studied high-penetration scenario. Although optimized pricing can reshape the spatial allocation of charging demand, the feeder still lacks sufficient voltage-support capability when no reactive resource is available.

By contrast, both support cases obtain feasible solutions in the representative evening hours. This indicates that distributed PV inverter reactive support restores the voltage-feasible operating region. Therefore, the primary function of reactive support is feasibility restoration rather than service optimization. Dynamic pricing can improve service and economic performance only after the physical voltage-security boundary has been recovered.

To further compare the two feasible support cases, the voltage profiles under fixed pricing with support and coordinated pricing with support are shown separately. The two supported cases both satisfy the voltage-security requirement, but coordinated pricing modifies the load distribution and slightly changes the voltage profile within the feasible operating region.

B. COORDINATED PRICING PERFORMANCE WITHIN THE FEASIBLE REGION

After feeder feasibility is restored by reactive support, coordinated pricing further improves operational performance. Relative to fixed pricing with support, the proposed coordinated strategy increases operator profit and reduces the average expected waiting burden in all three representative evening hours. The aggregate variations of charging load, expected waiting burden, minimum voltage, and profit are shown in Figure 8.

The representative-hour numerical comparison is given in Table II. At 17:00, the charging load increases by 6.79%, the average expected waiting burden decreases by 19.91%, feeder loss decreases by 21.75%, and operator profit increases by 41.36%. At 18:00, the charging load increases by 0.86%, the waiting burden decreases by 34.62%, feeder loss decreases by 37.40%, and operator profit increases by 37.90%. At 19:00, the charging load decreases by 2.26%, the waiting burden decreases by 23.18%, feeder loss decreases by 12.23%, and operator profit increases by 35.93%.

These results show that coordinated pricing does not simply increase or decrease total charging demand. Instead, it reallocates charging demand across stations in a way that improves service efficiency and operator-side benefit while preserving feeder feasibility. The minimum voltage remains within the admissible range, which indicates that the performance improvement is achieved inside the restored

Algorithm 1 **Rolling coordinated pricing and reactive-support optimization**

Initialize EV mobility states, SOC states, charger-availability states, and feeder states.
for each operating hour $t = 1, \ldots, T$ do
Observe the current system state Ω_t, including EV states, charger states, baseline load, and PV output.
Generate candidate station-wise price vectors within the admissible price bounds.
for each candidate price vector $\boldsymbol{\pi}_t$ do
Identify charging candidates according to the SOC threshold.
Construct the feasible station set for each charging candidate based on reachability and dwell-time constraints.
Calculate the generalized utility of each feasible station.
Determine station-choice probabilities using the logit model.
Simulate station selection, charger assignment, queue evolution, and charger-state carryover.
Aggregate station-level charging energy and calculate station-level charging loads.
Map station-level charging loads to the corresponding feeder buses.
Solve the SOCP-based feeder OPF with PV inverter reactive support.
if the SOCP OPF is feasible then
Set $\chi_t = 1$, and record feeder loss, voltage-deviation severity, and reactive-power dispatch.
Calculate the normalized objective value of the candidate.
else
Set $\chi_t = 0$, and add the infeasibility penalty to the candidate objective value.
end if
end for
Select the candidate price vector with the minimum penalized objective value.
Implement the selected price vector and the corresponding reactive-support dispatch.
Update the charging-service state and obtain Ω_{t+1}.
end for

TABLE 1. System configuration of the case study

Parameter	Value
Road network nodes	29
Charging stations	11
Trip records	25,527
Distribution nodes	33
Branch count	32
Battery capacity	60kWh
Target SOC	0.9
Equivalent implementation coefficient β_p	-1.2
Equivalent implementation coefficient β_t	-0.7
Equivalent implementation coefficient β_t	-0.2
Equivalent implementation coefficient β_w	-0.5
Voltage safety range	0.95–1.05 p.u.
PV buses	18, 22, 24, 29, 30, 32
PV rated power per bus	1500 kW
Inverter rating per bus	2250 kVA
Night-time reactive support	Enabled

TABLE 2. Representative-hour comparison relative to fixed pricing with support

Hour	Users	Load chg. (%)	Waiting-burden chg. (%)	Loss chg. (%)	Profit chg. (%)
17:00	235	6.79	-19.91	-21.75	41.36
18:00	264	0.86	-34.62	-37.40	37.90
19:00	243	-2.26	-23.18	-12.23	35.93

secure operating region rather than at the expense of voltage security.

C. STATION-LEVEL PRICE DIFFERENTIATION AND LOAD MIGRATION

The station-level results reveal how dynamic pricing reshapes charging-load allocation. The optimized prices differ across stations and hours, which indicates that the proposed method does not perform uniform tariff adjustment. Instead,

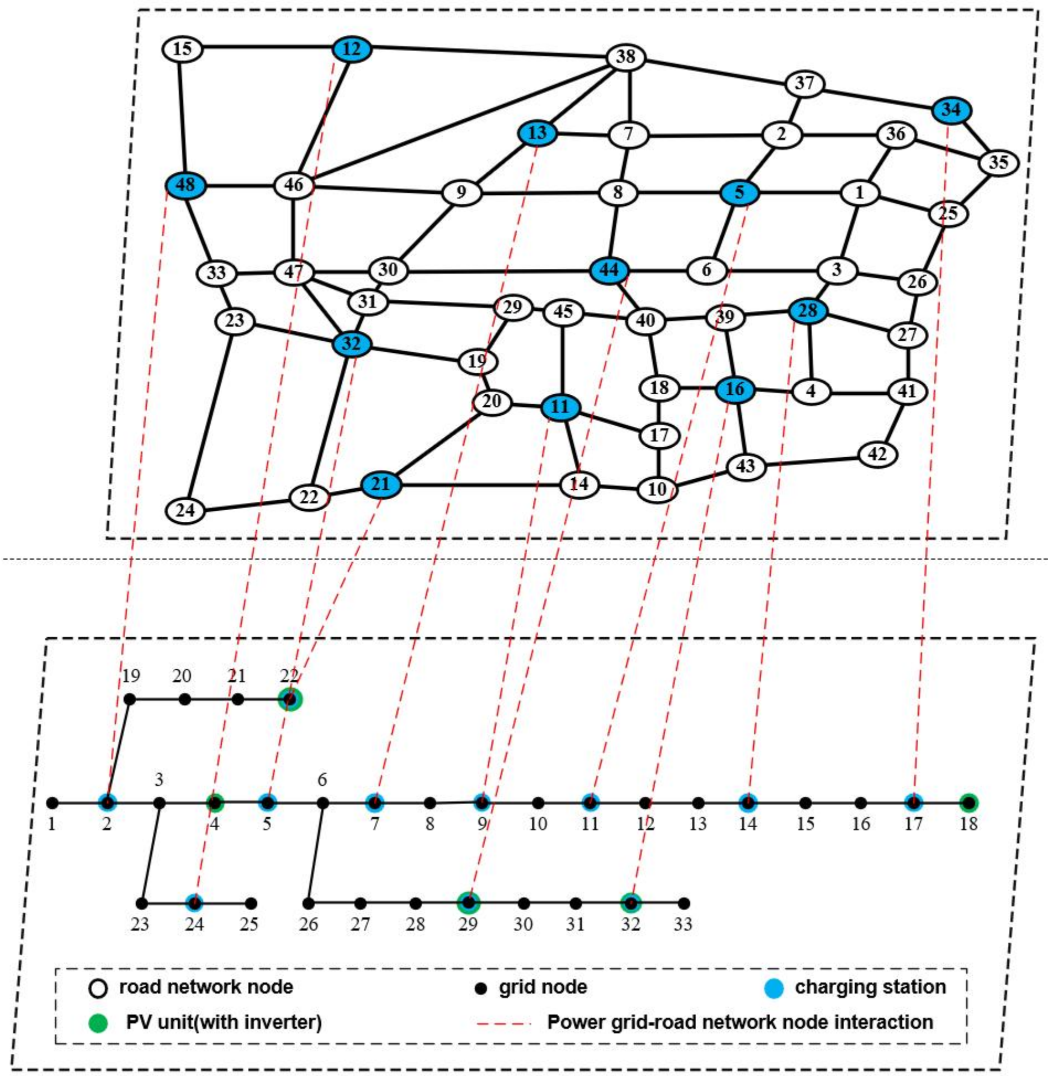

FIGURE 5. Coupled transportation–charging–distribution system used in the case study.

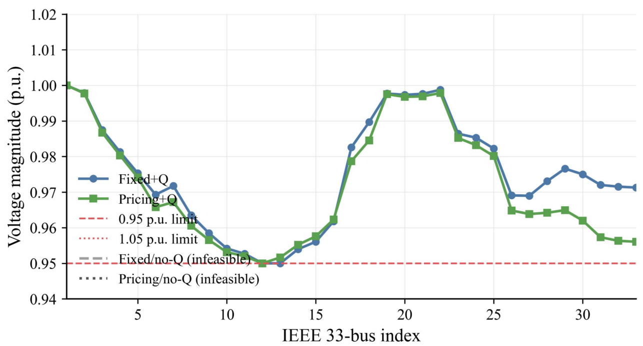

FIGURE 6. Voltage profile at 18:00 under four pricing-support cases.

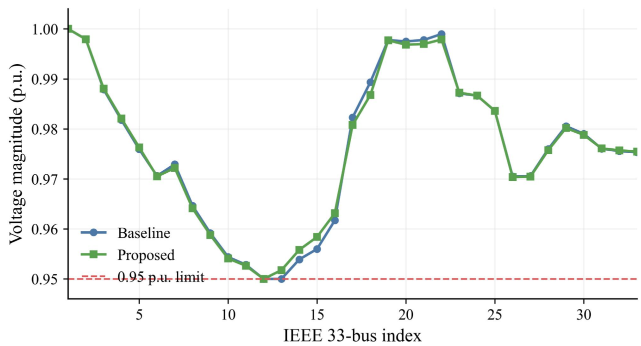

FIGURE 7. Voltage profile at 18:00 under fixed pricing with support and coordinated pricing with support.

it uses station-wise price differentiation to change the relative attractiveness of charging stations.

The corresponding station-hour load changes are shown in Figure 10. Positive values indicate that a station receives more charging demand under coordinated pricing than under fixed pricing, while negative values indicate that part of the demand is shifted away from the station.

The station-level numerical results are listed in Table III. These results show that the induced load migration is

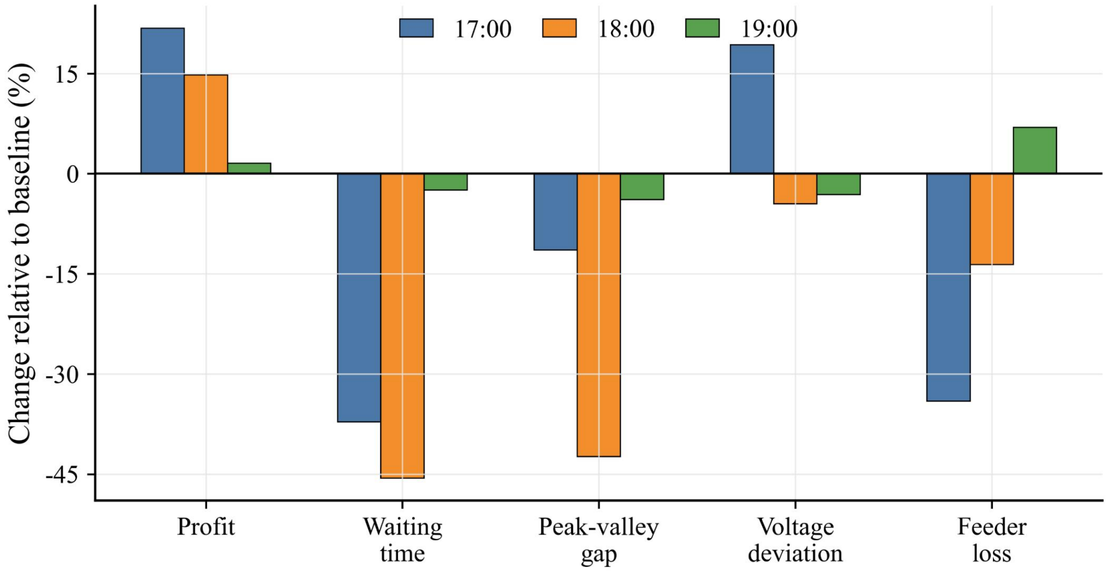

FIGURE 8. Aggregate performance comparison under fixed and coordinated pricing with reactive support.

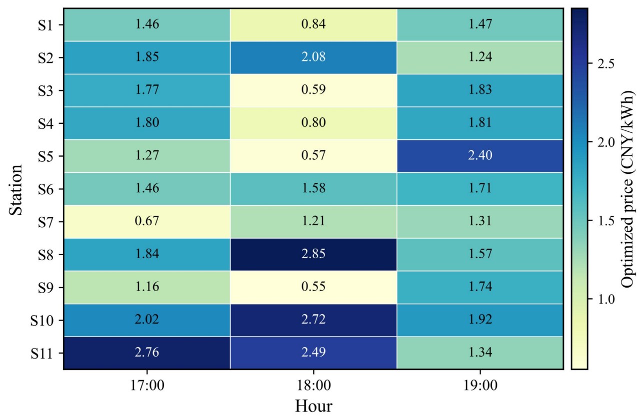

FIGURE 9. Station-wise optimized charging prices for the representative hours.

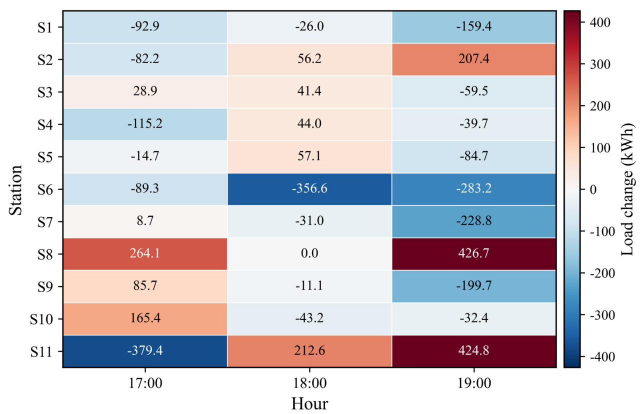

FIGURE 10. Station-hour charging-load changes under optimized pricing relative to fixed pricing.

not determined by price alone. Instead, users respond to the generalized burden that combines charging payment, travel time, charging duration, and expected waiting time. For example, at 17:00, the price of S10 increases from 2.00 CNY/kWh to 2.11 CNY/kWh, while its charging load increases from 206.08 kWh to 420.54 kWh. This result does not contradict the price-response logic, because the station-choice model is not based only on charging payment. If a station provides a lower expected waiting burden or better service accessibility, users may still select it even when the price is higher.

At the same hour, the charging load of S11 decreases from 369.94 kWh to 96.19 kWh, and its waiting burden decreases from 19.37 min to 5.00 min. This indicates that the coordinated strategy relieves local congestion by redirecting part of the demand away from overloaded service points. At 18:00 and 19:00, additional charging demand is shifted to S2 and S11. These station-level changes demonstrate that the proposed method performs spatial load migration rather than uniform price adjustment. The optimized price vector modifies the relative attractiveness of stations, while queue dynamics determine how the service burden evolves after users are reassigned. Therefore, the observed load redistribution is a joint outcome of price differentiation, waiting-time anticipation, and charger-state carryover.

D. ABLATION STUDY AND ALTERNATIVE STRATEGY COMPARISON

The ablation and alternative-strategy comparison is used to verify whether the proposed method provides a balanced operational compromise. Several simplified strategies improve one metric more strongly than the proposed method, but they often degrade other indicators. The results are summarized in Table IV. For example, queue-only pricing can reduce waiting burden significantly, but it increases feeder loss and worsens the station-load peak–valley gap. Without grid

TABLE 3. Representative station-level mechanism under coordinated pricing

Hour	Station (bus)	Price base	Price optimized	Load base (kWh)	Load optimized (kWh)	Waiting base (min)	Waiting optimized (min)
17:00	S10(32)	2.00	2.11	206.08	420.54	5.00	5.00
17:00	S11(12)	1.50	1.76	369.94	96.19	19.37	5.00
18:00	S2(22)	1.20	1.84	0.00	82.78	45.54	5.62
18:00	S11(12)	1.50	1.77	181.43	465.26	20.18	5.93
19:00	S2(22)	1.20	1.94	0.00	185.18	44.13	18.25
19:00	S11(12)	1.50	1.96	74.86	534.19	22.15	11.48

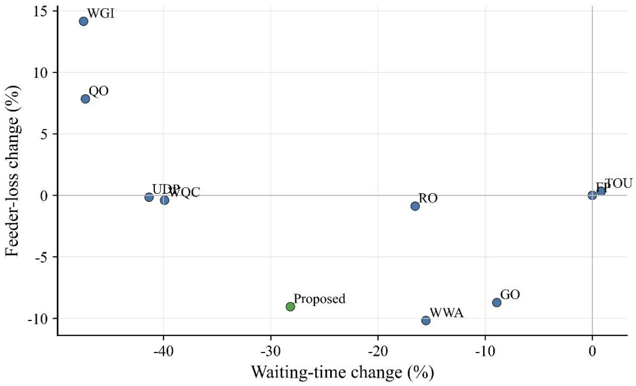

FIGURE 11. Trade-off between waiting-burden reduction and feeder-loss variation for alternative pricing strategies.

indicators, the operator profit and waiting-burden reduction are improved, but feeder loss increases by 14.15% and the peak–valley gap increases by 20.34%. These results show that optimizing only service-side indicators can move charging demand toward electrically unfavorable regions of the feeder.

The proposed method improves operator profit by 37.74%, reduces average expected waiting burden by 28.18%, decreases feeder loss by 9.03%, narrows the peak–valley gap by 24.46%, slightly reduces voltage-deviation severity by 0.52%, and increases served charging energy by 6.23%. These results indicate that the proposed strategy does not maximize a single indicator. Instead, it balances service quality, economic benefit, load distribution, and feeder operation.

The trade-off between waiting-burden reduction and feeder-loss variation is shown in Figure 11. Strategies that focus strongly on waiting-time reduction may lead to less favorable feeder-side performance. By contrast, the proposed method achieves a more balanced location in the trade-off space because feeder indicators are explicitly included in the objective function.

E. USER-SIDE TRADE-OFF AND SENSITIVITY ANALYSIS

The coordinated strategy also introduces a user-side trade-off. The average charging payment increases by 16.58%, the 95th-percentile payment increases by 9.49%, and the average generalized burden increases by 11.23%. These results should be reported explicitly because coordinated pricing improves operator-side and feeder-side indicators partly by changing user payment and station-selection incentives. Therefore, the proposed method should not be described as uniformly beneficial to all stakeholders. A more appropriate interpretation is that coordinated pricing improves system-level operation while introducing measurable user-side cost changes.

The sensitivity analysis is summarized in Table V. The tested factors include price upper bound, price-sensitivity coefficient, waiting-time sensitivity coefficient, charger number, and grid weight. The sensitivity results show that the main directional conclusions remain consistent under the tested parameter variations. Changes in price bounds, price-sensitivity coefficients, waiting-time sensitivity coefficients, charger numbers, and grid weights affect the numerical magnitude of the improvements, but the coordinated strategy generally maintains positive effects on profit, waiting burden, and feeder-side indicators. This suggests that the proposed framework is not tied to a single parameter setting.

Nevertheless, the sensitivity results also show that the trade-off among profit, waiting time, feeder loss, and served energy can shift under different behavioral and infrastructure assumptions. Therefore, the weighting coefficients and pricing bounds should be calibrated according to the operational priorities of the charging operator and distribution-network operator.

TABLE 4. Alternative-strategy and ablation comparison relative to fixed pricing with support

Strategy	Profit change (%)	Waiting-burden change (%)	Feeder-loss change (%)	Peak–valley-gap change (%)	Voltage-deviation change (%)	Served-energy change (%)
Fixed price	0.00	0.00	0.00	0.00	0.00	0.00
Time-of-use price	10.00	0.83	0.33	0.16	0.22	-1.17
Uniform dynamic price	22.20	-41.36	-0.14	38.20	3.37	31.47
Revenue-oriented heuristic	12.69	-16.53	-0.87	-4.87	-0.72	4.94
Queue-only pricing	11.20	-47.28	7.85	22.72	1.83	23.44
Grid-only pricing	37.92	-8.91	-8.71	-7.09	-0.30	4.46
Without queue carryover	14.54	-39.91	-0.39	2.61	-4.04	15.53
Without waiting anticipation	15.92	-15.53	-10.16	-24.02	-1.16	1.51
Without grid indicators	40.73	-47.46	14.15	20.34	-1.26	24.27
Proposed method	37.74	-28.18	-9.03	-24.46	-0.52	6.23

TABLE 5. Sensitivity analysis within the audited experiment scope

Factor	Setting	Profit change (%)	Waiting-time change (%)	Feeder-loss change (%)	Peak-gap change (%)	Voltage-deviation change (%)	Served-energy change (%)
Price upper bound	1.5x baseline	42.81	-28.49	-5.81	-11.68	-3.60	5.59
Price sensitivity	$\beta_p = -0.8$	34.84	-37.30	-4.27	-13.11	-2.88	11.41
Price sensitivity	$\beta_p = -1.2$	49.38	-29.77	-7.44	-20.30	0.18	3.59
Price sensitivity	$\beta_p = -1.6$	26.68	-23.00	-8.97	-17.82	-0.95	2.15
Waiting-time sensitivity	$\beta_w = -0.3$	15.92	-22.56	-12.69	-29.39	1.27	-0.18
Waiting-time sensitivity	$\beta_w = -0.5$	14.88	-31.40	-5.99	-16.91	-3.80	4.50
Waiting-time sensitivity	$\beta_w = -0.8$	16.95	-34.51	-8.50	-16.47	-2.18	7.77
Charger number	-20%	52.06	-5.62	-9.87	-6.10	-0.95	-3.22
Charger number	Baseline	24.57	-21.29	-9.46	-7.09	-1.85	3.36
Charger number	+20%	26.94	-33.10	-5.32	-19.46	-3.59	8.48
Grid weight	0.5x	19.32	-28.64	-7.81	-25.63	-0.19	3.74
Grid weight	1.0x	10.95	-15.55	-5.99	-19.52	-1.28	3.96
Grid weight	2.0x	17.65	-19.13	-4.19	-14.52	-2.47	3.77

VII. CONCLUSION

This paper develops a coordinated rolling optimization framework for EV charging pricing and distributed photovoltaic inverter reactive support in high-penetration source–load distribution networks. The proposed framework links utility-based station choice, queue-aware charging-service simulation, station-to-bus load mapping, and SOCP-based feeder-security evaluation. Different from conventional formulations that treat EV charging demand as an exogenous load profile, the proposed model describes station-level charging demand as an endogenous result of user response, price signals, charger availability, and queue carryover.

The case studies show that dynamic pricing and distributed reactive support play different but complementary roles. Pricing alone cannot recover feeder security under representative evening peak conditions, because price-guided load migration may still lead to voltage-infeasible operating points. Distributed photovoltaic inverter reactive support restores the voltage-feasible operating region under the 0.95–1.05 p.u. security requirement. Within this recovered secure region, dynamic pricing further reshapes station-level charging demand to improve service quality and operator-side benefit. Compared with fixed pricing with reactive support, the proposed strategy increases full-day operator profit by 37.74%, reduces average expected waiting burden by 28.18%, decreases feeder loss by 9.03%, narrows the station-load peak–valley gap by 24.46%, slightly reduces voltage-deviation severity by 0.52%, and increases served charging energy by 6.23%.

The results also reveal an important user-side trade-off. Although the coordinated strategy improves system-level operation, it increases average charging payment, the 95th-percentile payment, and the average generalized user burden. Therefore, the proposed method should not be interpreted as a uniformly beneficial pricing rule for all stakeholders. A more appropriate interpretation is that distributed reactive support provides the physical feasibility margin, while dynamic pricing reallocates charging demand within this margin to balance operator profit, service efficiency, load distribution, and feeder operation.

ACKNOWLEDGMENT

This research was funded by State Grid Co., Ltd. Science and Technology Project (kj2025-033).

REFERENCES

[1] M. Xylia, E. Olsson, B. Macura, and B. Nykvist, “Estimating charging infrastructure demand for electric vehicles: a systematic review,” Energy Strategy Reviews, vol. 59, Art. no. 101753, 2025.

[2] F. Ahmed, S. Ahmad, M. T. Rahman, M. R. Hazari, R. Faiz, T. Ahmed, and M. Karimi, “A holistic review of electric vehicle charging impacts on power distribution networks: Technical challenges, smart mitigation strategies and future directions,” Applied Energy, vol. 402, Art. no. 126961, 2026.

[3] J. Tian, S. Li, K. Wang, Z. Zheng, and Q. Zhang, “Data-driven analysis of ev public charging station demand across heterogeneous built environment,” Transportation Research Part D: Transport and Environment, vol. 158, Art. no. 105455, 2026.

[4] C. Wang, F. He, X. Lin, Z.-J. M. Shen, and M. Li, “Designing locations and capacities for charging stations to support intercity travel of electric vehicles: An expanded network approach,” Transportation Research Part C: Emerging Technologies, vol. 102, pp. 210–232, 2019.

[5] X. Chen, Z. Lei, and S. V. Ukkusuri, “Modeling the influence of charging cost on electric ride-hailing vehicles,” Transportation Research Part C: Emerging Technologies, vol. 160, Art. no. 104514, 2024.

[6] Y. Wen, D. MacKenzie, and D. R. Keith, “Modeling the charging choices of battery electric vehicle drivers by using stated preference data,” Transportation Research Record: Journal of the Transportation Research Board, vol. 2572, no. 1, pp. 47–55, 2016.

[7] H. Wu, X. Lan, Y. He, A. Y. Wu, and M. Ding, “Orderly charging of electric vehicles: A two-stage spatial-temporal scheduling method based on user-personalized navigation,” Applied Energy, vol. 378, Art. no. 124800, 2025.

[8] J. Vuelvas, F. Ruiz, and G. Gruosso, “A time-of-use pricing strategy for managing electric vehicle clusters,” Sustainable Energy, Grids and Networks, vol. 25, Art. no. 100411, 2021.

[9] L. Cui, Q. Wang, H. Qu, M. Wang, Y. Wu, and L. Ge, “Dynamic pricing for fast charging stations with deep reinforcement learning,” Applied Energy, vol. 346, Art. no. 121334, 2023.

[10] R. Cheng, G. Liu, W. Liu, Q. Shi, and Q. Chen, “A personalized network-aware price design for electric vehicle charging using a sequential stackelberg game,” Applied Energy, vol. 381, Art. no. 125145, 2025.

[11] K. N. Hasan, K. M. Muttaqi, P. Borbora, J. Scira, Z. Zhang, and M. Leishman, “Distribution network voltage analysis with data-driven electric vehicle load profiles,” Sustainable Energy, Grids and Networks, vol. 36, Art. no. 101216, 2023.
[12] T. Theodoropoulos, P. Pantazopoulos, E. Karfopoulos, P. Lytrivis, G. Karaseitanidis, and A. Amditis, “Proportionally fair and scalable ev charging under distribution line voltage constraints,” Electric Power Systems Research, vol. 208, Art. no. 107797, 2022.
[13] S. Lee and D.-H. Choi, “Dynamic pricing and energy management for profit maximization in multiple smart electric vehicle charging stations: A privacy-preserving deep reinforcement learning approach,” Applied Energy, vol. 304, Art. no. 117754, 2021.
[14] S. Bae, B. Kulcsar, and S. Gros, “Personalized dynamic pricing policy for electric vehicles: Reinforcement learning approach,” Transportation Research Part C: Emerging Technologies, vol. 161, Art. no. 104540, 2024.
[15] M. Tahmasebi, A. Ghadiri, M. R. Haghifam, and S. M. Miri-Larimi, “Mpc-based approach for online coordination of evs considering ev usage uncertainty,” International Journal of Electrical Power & Energy Systems, vol. 130, Art. no. 106931, 2021.
[16] B. Khaki, Y. Chung, C. Chu, and R. Gadh, “Hierarchical distributed framework for ev charging scheduling using exchange problem,” Applied Energy, vol. 241, pp. 461–471, 2019.
[17] E. Xydas, C. Marmaras, and L. M. Cipcigan, “A multi-agent based scheduling algorithm for adaptive electric vehicles charging,” Applied Energy, vol. 177, pp. 354–365, 2016.
[18] M. Schmidt, P. Staudt, and C. Weinhardt, “Evaluating the importance and impact of user behavior on public destination charging of electric vehicles,” Applied Energy, vol. 258, Art. no. 114061, 2020.
[19] D. Yang, N. J. S. Sarma, M. F. Hyland, and R. Jayakrishnan, “Dynamic modeling and real-time management of a system of ev fast-charging stations,” Transportation Research Part C: Emerging Technologies, vol. 128, Art. no. 103186, 2021.
[20] O. B. Kiray, F. Gzara, and S. A. Alumur, “Charging station location and sizing for electric vehicles under congestion,” Transportation Science, vol. 57, no. 6, pp. 1433–1451, 2023.
[21] F. G. Quilici, G. Lutzemberger, A. Ruvio, C. Scarpelli, M. Lagnoni, and A. Bertei, “How fast is fast? sizing and simulation of ev charging stations under operational uncertainty,” Energy Conversion and Management: X, vol. 30, Art. no. 101737, 2026.
[22] A. M. A. Haidar and K. M. Muttaqi, “Behavioral characterization of electric vehicle charging loads in a distribution power grid through modeling of battery chargers,” IEEE Transactions on Industry Applications, vol. 52, no. 1, pp. 483–492, 2016.
[23] N. H. Tehrani and P. Wang, “Probabilistic estimation of plug-in electric vehicles charging load profile,” Electric Power Systems Research, vol. 124, pp. 133–143, 2015.
[24] L. Bobo, A. Venzke, and S. Chatzivasileiadis, “Second-order cone relaxations of the optimal power flow for active distribution grids: Comparison of methods,” International Journal of Electrical Power & Energy Systems, vol. 127, Art. no. 106625, 2021.
[25] R. Haider and A. M. Annaswamy, “A hybrid architecture for volt-var control in active distribution grids,” Applied Energy, vol. 312, Art. no. 118735, 2022.
[26] D. Mak, D. Choeum, and D.-H. Choi, “Sensitivity analysis of volt-var optimization to data changes in distribution networks with distributed energy resources,” Applied Energy, vol. 261, Art. no. 114331, 2020.
[27] M. Farivar and S. H. Low, “Branch flow model: Relaxations and convexification—part i,” IEEE Transactions on Power Systems, vol. 28, no. 3, pp. 2554–2564, 2013.
[28] S. H. Low, “Convex relaxation of optimal power flow—part i: Formulations and equivalence,” IEEE Transactions on Control of Network Systems, vol. 1, no. 1, pp. 15–27, 2014.
[29] L. Collins and J. K. Ward, “Real and reactive power control of distributed pv inverters for overvoltage prevention and increased renewable generation hosting capacity,” Renewable Energy, vol. 81, pp. 464–471, 2015.
[30] P. A. V. Pato, F. C. L. Trindade, and X. Wang, “Hosting high pv penetration on distribution feeders with smart inverters providing local var compensation,” Electric Power Systems Research, vol. 217, Art. no. 109168, 2023.
[31] R. K. Varma and E. M. Siavashi, “Pv-statcom: A new smart inverter for voltage control in distribution systems,” IEEE Transactions on Sustainable Energy, vol. 9, no. 4, pp. 1681–1691, 2018.
[32] A. Zecchino and M. Marinelli, “Analytical assessment of voltage support via reactive power from new electric vehicles supply equipment in radial distribution grids with voltage-dependent loads,” International Journal of Electrical Power & Energy Systems, vol. 97, pp. 17–27, 2018.
[33] J. Stiasny, T. Zufferey, G. Pareschi, D. Toffanin, G. Hug, and K. Boulouchos, “Sensitivity analysis of electric vehicle impact on low-voltage distribution grids,” Electric Power Systems Research, vol. 191, Art. no. 106696, 2021.
[34] S. Xie, Z. Hu, and J. Wang, “Scenario-based comprehensive expansion planning model for a coupled transportation and active distribution system,” Applied Energy, vol. 255, Art. no. 113782, 2019.
[35] L. Geng, Z. Lu, L. He, J. Zhang, X. Li, and X. Guo, “Smart charging management system for electric vehicles in coupled transportation and power distribution systems,” Energy, vol. 189, Art. no. 116275, 2019.
[36] L. Sun and D. Lubkeman, “Agent-based modeling of feeder-level electric vehicle diffusion for distribution planning,” IEEE Transactions on Smart Grid, vol. 12, no. 1, pp. 751–760, 2021.
[37] Y. Xiang, J. Liu, R. Li, F. Li, C. Gu, and S. Tang, “Economic planning of electric vehicle charging stations considering traffic constraints and load profile templates,” Applied Energy, vol. 178, pp. 647–659, 2016.
[38] Y. Song, D. Ngoduy, T. Dantsuji, and C. Ding, “Dynamic equilibrium of the coupled transportation and power networks considering electric vehicles charging behavior,” Transportation Research Part A: Policy and Practice, vol. 199, Art. no. 104590, 2025.
[39] Z. Liu and Z. Song, “Network user equilibrium of battery electric vehicles considering flow-dependent electricity consumption,” Transportation Research Part C: Emerging Technologies, vol. 95, pp. 516–544, 2018.
[40] A. Pal, A. Bhattacharya, and A. K. Chakraborty, “Planning of ev charging station with distribution network expansion considering traffic congestion and uncertainties,” IEEE Transactions on Industry Applications, vol. 59, no. 3, pp. 3810–3825, 2023.
[41] Y. Zheng, Z. Y. Dong, Y. Xu, K. Meng, J. H. Zhao, and J. Qiu, “Electric vehicle battery charging/swap stations in distribution systems: Comparison study and optimal planning,” IEEE Transactions on Power Systems, vol. 29, no. 1, pp. 221–229, 2014.